



---

Year: 2022

---

## Quantum Iterative Reconstruction for Abdominal Photon-counting Detector CT Improves Image Quality

Sartoretti, Thomas ; Landsmann, Anna ; Nakhostin, Dominik ; Eberhard, Matthias ; Röeren, Christian ; Mergen, Victor ; Higashigaito, Kai ; Raupach, Rainer ; Alkadhi, Hatem ; Euler, André

**Abstract:** Background An iterative reconstruction (IR) algorithm was introduced for clinical photon-counting detector (PCD) CT. Purpose To investigate the image quality and the optimal strength level of a quantum IR algorithm (QIR; Siemens Healthcare) for virtual monoenergetic images and polychromatic images (T3D) in a phantom and in patients undergoing portal venous abdominal PCD CT. Materials and Methods In this retrospective study, noise power spectrum (NPS) was measured in a water-filled phantom. Consecutive oncologic patients who underwent portal venous abdominal PCD CT between March and April 2021 were included. Virtual monoenergetic images at 60 keV and T3D were reconstructed without QIR (QIR-off; reference standard) and with QIR at four levels (QIR 1-4; index tests). Global noise index, contrast-to-noise ratio (CNR), and voxel-wise CT attenuation differences were measured. Noise and texture, artifacts, diagnostic confidence, and overall quality were assessed qualitatively. Conspicuity of hypodense liver lesions was rated by four readers. Parametric (analyses of variance, paired t tests) and nonparametric tests (Friedman, post hoc Wilcoxon signed-rank tests) were used to compare quantitative and qualitative image quality among reconstructions. Results In the phantom, NPS showed unchanged noise texture across reconstructions with maximum spatial frequency differences of 0.01 per millimeter. Fifty patients (mean age, 59 years  $\pm$  16 [standard deviation]; 31 women) were included. Global noise index was reduced from QIR-off to QIR-4 by 45% for 60 keV and by 44% for T3D (both,  $P < .001$ ). CNR of the liver improved from QIR-off to QIR-4 by 74% for 60 keV and by 69% for T3D (both,  $P < .001$ ). No evidence of difference was found in mean attenuation of fat and liver ( $P = .79-.84$ ) and on a voxel-wise basis among reconstructions. Qualitatively, QIR-4 outperformed all reconstructions in every category for 60 keV and T3D ( $P$  value range,  $<.001$  to  $.01$ ). All four readers rated QIR-4 superior to other strengths for lesion conspicuity ( $P$  value range,  $<.001$  to  $.04$ ). Conclusion In portal venous abdominal photon-counting detector CT, an iterative reconstruction algorithm (QIR; Siemens Healthcare) at high strength levels improved image quality by reducing noise and improving contrast-to-noise ratio and lesion conspicuity without compromising image texture or CT attenuation values. © RSNA, 2022 Online supplemental material is available for this article. See also the editorial by Sinitsyn in this issue.

DOI: <https://doi.org/10.1148/radiol.211931>

Posted at the Zurich Open Repository and Archive, University of Zurich

ZORA URL: <https://doi.org/10.5167/uzh-217069>

Journal Article

Published Version



The following work is licensed under a Creative Commons: Attribution 4.0 International (CC BY 4.0) License.

Originally published at:

Sartoretti, Thomas; Landsmann, Anna; Nakhostin, Dominik; Eberhard, Matthias; Röeren, Christian; Mergen, Victor; Higashigaito, Kai; Raupach, Rainer; Alkadhi, Hatem; Euler, André (2022). Quantum Iterative Reconstruction for Abdominal Photon-counting Detector CT Improves Image Quality. *Radiology*, 303(2):339-348.  
DOI: <https://doi.org/10.1148/radiol.211931>



# Quantum Iterative Reconstruction for Abdominal Photon-counting Detector CT Improves Image Quality

Thomas Sartoretti, BMed • Anna Landsmann, MD • Dominik Nakhostin, MD • Matthias Eberhard, MD, EBCR • Christian Roeren, MD • Victor Mergen, MD • Kai Higashigaito, MD • Rainer Raupach, PhD • Hatem Alkadhi, MD, MPH, EBCR, FESER • André Euler, MD

From the Institute of Diagnostic and Interventional Radiology, University Hospital Zurich, University of Zurich, Raemistrasse 100, CH-8091 Zurich, Switzerland (T.S., A.L., D.N., M.E., C.R., V.M., K.H., H.A., A.E.); Department of Radiology and Nuclear Medicine, Maastricht University Medical Center, Maastricht University, Maastricht, the Netherlands (T.S.); and Siemens Healthcare, Forchheim, Germany (R.R.). Received July 30, 2021; revision requested September 21; revision received November 11; accepted November 24. **Address correspondence to** A.E. (e-mail: [andre.euler@usz.ch](mailto:andre.euler@usz.ch)).

Conflicts of interest are listed at the end of this article.

See also the editorial by Sinitsyn in this issue.

Radiology 2022; 303:339–348 • <https://doi.org/10.1148/radiol.211931> • Content codes:  

**Background:** An iterative reconstruction (IR) algorithm was introduced for clinical photon-counting detector (PCD) CT.

**Purpose:** To investigate the image quality and the optimal strength level of a quantum IR algorithm (QIR; Siemens Healthcare) for virtual monoenergetic images and polychromatic images (T3D) in a phantom and in patients undergoing portal venous abdominal PCD CT.

**Materials and Methods:** In this retrospective study, noise power spectrum (NPS) was measured in a water-filled phantom. Consecutive oncologic patients who underwent portal venous abdominal PCD CT between March and April 2021 were included. Virtual monoenergetic images at 60 keV and T3D were reconstructed without QIR (QIR-off; reference standard) and with QIR at four levels (QIR 1–4; index tests). Global noise index, contrast-to-noise ratio (CNR), and voxel-wise CT attenuation differences were measured. Noise and texture, artifacts, diagnostic confidence, and overall quality were assessed qualitatively. Conspicuity of hypodense liver lesions was rated by four readers. Parametric (analyses of variance, paired *t* tests) and nonparametric tests (Friedman, post hoc Wilcoxon signed-rank tests) were used to compare quantitative and qualitative image quality among reconstructions.

**Results:** In the phantom, NPS showed unchanged noise texture across reconstructions with maximum spatial frequency differences of 0.01 per millimeter. Fifty patients (mean age, 59 years  $\pm$  16 [standard deviation]; 31 women) were included. Global noise index was reduced from QIR-off to QIR-4 by 45% for 60 keV and by 44% for T3D (both,  $P < .001$ ). CNR of the liver improved from QIR-off to QIR-4 by 74% for 60 keV and by 69% for T3D (both,  $P < .001$ ). No evidence of difference was found in mean attenuation of fat and liver ( $P = .79$ –.84) and on a voxel-wise basis among reconstructions. Qualitatively, QIR-4 outperformed all reconstructions in every category for 60 keV and T3D ( $P$  value range,  $<.001$  to  $.01$ ). All four readers rated QIR-4 superior to other strengths for lesion conspicuity ( $P$  value range,  $<.001$  to  $.04$ ).

**Conclusion:** In portal venous abdominal photon-counting detector CT, an iterative reconstruction algorithm (QIR; Siemens Healthcare) at high strength levels improved image quality by reducing noise and improving contrast-to-noise ratio and lesion conspicuity without compromising image texture or CT attenuation values.

© RSNA, 2022

Online supplemental material is available for this article.

An earlier incorrect version appeared online and in print. This article was corrected online on June 27, 2022.

A CT system that uses photon-counting detector (PCD) technology was released in 2021 for clinical use. Compared with previous energy-integrating detector CT systems, this first-generation dual-source full field-of-view PCD CT can detect and weigh single photons on the basis of their energies, enabling spectral separation and multi-material decomposition (1–3). Prototype PCD CT systems have been shown to provide improved spatial resolution, dose efficiency, contrast-to-noise ratio (CNR), and lower image noise (4–12).

Whereas hardware improvements are critical to ensure high-quality CT, image reconstruction techniques also contribute decisively toward image quality and perception. In the last 2 decades, iterative reconstruction (IR) became the standard reconstruction technique for CT. IR overcomes the limitations of traditional filtered back projection by substantially

lowering image noise, especially in low signal conditions (13–17). Previously developed IRs are not optimal for PCD CT imaging because of a variety of technical factors such as increased data complexity, spectral information, and noise model (13).

With the introduction of PCD CT, the vendor introduced a quantum IR algorithm (QIR; Siemens Healthcare). QIR has four strength levels and is specifically tailored to PCD CT. In addition, given the multienergy capabilities of PCD CT, the routine reconstruction of virtual monoenergetic images as the reference standard for diagnostic readouts was defined (18,19).

The purpose of our study is to investigate the image quality and the optimal strength level of QIR for virtual monoenergetic images and polychromatic images (T3D) in a phantom and in patients at portal venous phase abdominal PCD CT.

## Abbreviations

CNR = contrast-to-noise ratio, IR = iterative reconstruction, NPS = noise power spectrum, PCD = photon-counting detector, T3D = polychromatic image

## Summary

High levels of quantum iterative reconstruction (QIR; Siemens Healthcare) reduced noise and improved contrast-to-noise ratio and lesion conspicuity without compromising image texture or CT attenuation values in portal venous abdominal photon-counting detector CT.

## Key Results

- In a retrospective study of 50 consecutive patients and a phantom, image noise was reduced by 45% and 44% and contrast-to-noise ratio (CNR) improved by 74% and 69% for the liver and portal vein, respectively, by using high strength levels of iterative reconstruction (QIR; Siemens Healthcare) and 60 keV in portal venous abdominal photon-counting detector CT.
- Higher strength levels of QIR improved lesion conspicuity and subjective image quality compared to QIR-off for 60-keV and polychromatic images.
- No difference was found for image texture and CT attenuation values among reconstructions (maximum deviation of 0.01 per millimeter spatial frequency and maximum mean attenuation difference of 2 HU for attenuation of the portal vein between two given reconstructions).

## Materials and Methods

One author (R.R.) is an employee of Siemens Healthcare (Forchheim, Germany). This author did not have control over the data at any point during the study.

### Phantom Parameters

A water-filled cylindrical container emulating an intermediate-sized patient (diameter, 30 cm) was scanned once with the same CT protocol and radiation dose as used in patients. Volume CT dose index, or  $CTDI_{vol}$ , was 6.5 mGy and dose-length product was 234 mGy · cm.

### Patient Inclusion

This study had institutional review board and local ethics committee approval. All patients provided written informed consent. Between March and April 2021, we retrospectively assessed 50 consecutive patients who were referred for oncologic follow-up imaging to our radiology department in an academic university hospital (Table 1, Fig 1). Inclusion criteria were age 18 years or older, multienergy CT protocol performed with a clinical PCD CT, and portal venous phase of the abdomen.

### Data Acquisition

Imaging was performed on a first-generation clinical dual-source PCD CT (Naotom Alpha; Siemens Healthcare) in the single-source, multi-energy mode (QuantumPlus; Siemens Healthcare) by using the following scan parameters: 120 kVp; detector collimation,  $144 \times 0.4$  mm (total of 57.6 mm); pitch, 0.8; and gantry rotation time, 0.5 second. Tube current–time product was adapted by using an image quality level of 100 for automatic exposure control. The image quality level represents quality reference milliampere-seconds. This denotes effective milliampere-seconds applied for the

**Table 1: Patient Demographics**

Characteristic	Value
No. of patients	50
Mean age (y)*	59 ± 16 (21–85)
Sex	
No. of women	31
No. of men	19
Mean body weight (kg)	72.6 ± 20
Mean body mass index (kg/m <sup>2</sup> )	25.2 ± 6.2
Mean height (cm)	170 ± 9
Mean effective diameter (cm)	28.7 ± 3.8
Indications for imaging	
Gastrointestinal tumor	12
Liver tumor	9
Hematologic neoplasia	5
Urogenital tumor	5
Lung tumor	4
Abscess/infection	5
Exploratory tumor search	3
Breast tumor	3
Pancreas tumor	1
Sarcoma	2
Intra-abdominal hematoma	1
Liver lesions <sup>†</sup>	
Hemangioma	6 (8 ± 3)
Cyst	5 (11 ± 9)
Metastasis <sup>‡</sup>	6 (19 ± 9)
Hepatocellular carcinoma	1 (35)

Note.—Unless otherwise indicated, data are numbers of patients or tumors. Mean data are ± standard deviation.

\* Data are mean; data in parentheses are range.

<sup>†</sup> Data in parentheses are mean millimeters of maximum diameter.

<sup>‡</sup> Four patients exhibited multiple liver metastases.

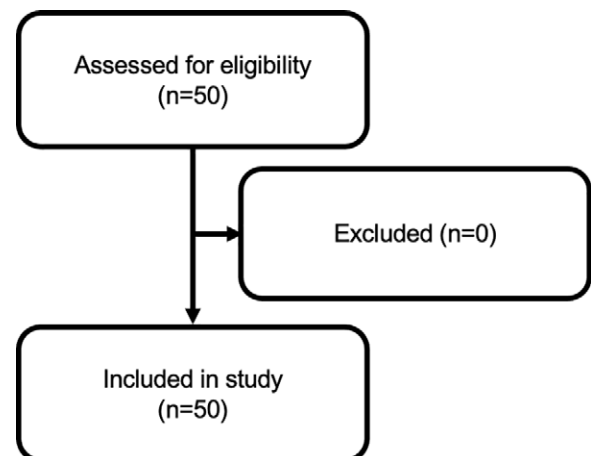


**Figure 1:** Patient inclusion flowchart.

protocol-specific reference water-equivalent diameter with a CT geometry correction, particularly for the effect of the focal spot to isocenter distance. Therefore, the image quality level provides a system- and reconstruction-independent image quality definition. Acquisition in the portal venous phase

**Table 2: Overview of Data from Quantitative Image Analysis among All Reconstructions**

Parameter	QIR-Off		QIR-1		QIR-2		QIR-3		QIR-4	
	60 keV	T3D	60 keV	T3D	60 keV	T3D	60 keV	T3D	60 keV	T3D
Global noise index (HU)	24.9 ± 3.7	20.6 ± 3.3	22 ± 3.3	18.5 ± 3.2	19.3 ± 3.0	16.1 ± 2.9	16.6 ± 2.7	13.8 ± 2.7	13.7 ± 2.3	11.4 ± 2.2
CNR Liver	11 ± 2.7	11.5 ± 2.5	12.3 ± 2.4	12.7 ± 2.9	13.9 ± 2.9	14.4 ± 3.4	16 ± 3.5	16.5 ± 4.2	19.1 ± 4.5	19.4 ± 5.3
CNR portal vein	4.4 ± 1.6	3.4 ± 1.6	5.0 ± 1.8	3.7 ± 1.6	5.6 ± 2.0	4.2 ± 1.8	6.4 ± 2.4	4.8 ± 2.1	7.5 ± 2.9	5.6 ± 2.5
Fat attenuation (HU)	-107 ± 17.7	-98.4 ± 15.4	-107 ± 17.6	-98.3 ± 15.3	-107 ± 17.6	-98.2 ± 15.3	-107 ± 17.6	-98.2 ± 15.3	-108 ± 18.4	-98.1 ± 15.3
Liver attenuation (HU)	128 ± 20.8	104 ± 15.6	128 ± 20.7	104 ± 15.6	128 ± 20.7	104 ± 15.6	128 ± 20.7	104 ± 15.6	128 ± 20.7	104 ± 15.7
Portal vein attenuation (HU)	223 ± 34.2	163 ± 21.3	223 ± 34.1	163 ± 21.3	223 ± 34.2	163 ± 21.3	222 ± 34.2	163 ± 21.4	221 ± 34.8	162 ± 21.4
Voxel-wise differences in attenuation (HU)	...	...	-0.03 ± 0.35	-0.02 ± 0.29	-0.06 ± 0.69	-0.04 ± 0.56	-0.08 ± 1.03	-0.05 ± 0.84	-0.11 ± 1.38	-0.07 ± 1.12
NPS magnitude (HU)	17.3	14.3	15.3	12.7	13.3	11	11.3	9.4	9.3	7.7
NPS $f_{av}$ (1/mm)	0.19	0.2	0.19	0.2	0.19	0.19	0.18	0.19	0.18	0.19
NPS $f_{peak}$ (1/mm)	0.14	0.16	0.14	0.16	0.14	0.16	0.14	0.16	0.14	0.16

Note.—Mean data are ± standard deviation. QIR is an iterative reconstruction algorithm from Siemens Healthcare. CNR = contrast-to-noise ratio,  $f_{av}$  = average spatial frequency,  $f_{peak}$  = peak spatial frequency, NPS = noise power spectrum, T3D = polychromatic images at photon-counting detector CT.

was performed with a delay of 70 seconds after injection of a weight-based iodinated contrast medium (370 mg of iodine per milliliter; Iopromidum, Ultravist, Bayer Healthcare). The average volume CT dose index, or  $CTDI_{vol}$ , was 6.6 mGy ± 4.2 (standard deviation) and the average dose-length product was 298.9 mGy · cm ± 139.7.

### Image Reconstruction

Two image types were reconstructed. First, virtual monoenergetic images at 60 keV by combining the counting data simultaneously acquired at different energy thresholds were reconstructed. These images represent the standard for abdominal imaging as specified by the vendor. Second, polychromatic images were reconstructed by using the data from all counted events above the lowest energy threshold at 20 keV (termed T3D for PCD CT). Despite the count weighting at PCD CT versus energy weighting at energy-integrating detector CT, T3D is most comparable to a conventional reconstruction with energy-integrating detector CT systems that accumulate all measured x-ray quanta without differentiating their energies.

Both image types were reconstructed on the axial plane without QIR (QIR-off) and with all strength levels of QIR (QIR 1–4). The following parameters were used: Br36 reconstruction kernel; section thickness, 2 mm; 1.6-mm increment; and matrix, 512 × 512 pixels.

Of note, standard filtered back projection algorithms are not suitable for the reconstruction of monoenergetic images because the retrieval of monoenergetic information from the threshold data may lead to amplification of image noise. Therefore, PCD CT does not offer a pure filtered back projection-type reconstruction algorithm for spectral results. Instead, QIR-off is available, in which minimally possible

statistical optimization is achieved compared with standard weighted filtered back projection.

QIR is an IR approach that corrects for geometric cone beam artifacts and performs a statistical optimization of spectral data. QIR strengths 1–4 trigger an additional statistical optimization in terms of a globally reduced target noise level for which higher strength levels correspond to stronger optimization (ie, greater noise reduction; Appendix E1 [online]).

### Quantitative Analysis

Metrics were computed separately for each image type (60 keV, T3D) and reconstruction (QIR-off and QIR 1–4). Figure E1 (online) is a visual representation of all quantitative analyses.

**Phantom.**—Noise power spectrum (NPS) was measured by using an open-source software (ImQuest Version 7; Duke University). Quadratic regions of interest with an area of approximately 16 cm<sup>2</sup> were placed in the center of the phantom on 100 consecutive sections. One-dimensional NPS profiles depicting the radial average of the two-dimensional NPS profile were generated. To compare the noise texture, the average and peak spatial frequencies of the NPS curves were compared.

**Patients.**—CNR (20) and CT attenuation were measured manually by one reader (D.N., in training with 3 years of experience in abdominal imaging). Measurements were performed in the liver parenchyma (right and left hepatic lobes), main portal vein at the level of the porta hepatis, and in the subcutaneous fat in the anterior abdominal wall at the level of the L3 vertebra. The global noise index (21) (representing a robust measure to quantify the noise level in vivo across all image sections of a single examination) and voxel-wise differ-

**Table 3: Overview of Data from Qualitative Image Analysis among All Reconstructions**

Parameter	QIR-Off		QIR-1		QIR-2		QIR-3		QIR-4	
	60 keV	T3D	60 keV	T3D	60 keV	T3D	60 keV	T3D	60 keV	T3D
Overall image quality										
Reader 1	3 (3–3)		3 (3–4)	4 (3–4)	4 (4–4)	4 (4–4)	4 (4–4)	4.5 (4–5)	5 (5–5)	5 (5–5)
Reader 2	3 (3–3)	3 (3–4)	3 (3–4)	4 (3–4)	4 (4–4)	4 (4–4)	5 (4–5)	5 (4–5)	5 (5–5)	5 (5–5)
Image artifacts and diagnostic confidence										
Reader 1	3 (3–3)	3 (3–3)	3 (3–4)	4 (3–4)	4 (4–4)	4 (4–4)	4 (4–4)	4.5 (4–5)	5 (5–5)	5 (5–5)
Reader 2	3 (3–3)	3 (3–3)	3 (3–4)	4 (3–4)	4 (4–4)	4 (4–4)	4 (4–5)	5 (4–5)	5 (4–5)	5 (5–5)
Image noise and texture										
Reader 1	–2 (–2 to –2)	–2 (–2 to –1)	–2 (–2 to –1)	–1 (–2 to –1)	–1 (–1 to –1)	–1 (–1 to –1)	–1 (–1 to –1)	–1 (–1 to 0)	–1 (–1 to 0)	0 (0–0)
Reader 2	–2 (–2 to –2)	–2 (–2 to –1)	–2 (–2 to –1)	–1 (–2 to –1)	–1 (–1 to –1)	–1 (–1 to –1)	–1 (–1 to –1)	–1 (–1 to 0)	–1 (–1 to 0)	0 (0–0)
Lesion conspicuity										
Reader 1	–2 (–2 to –2)	–2 (–2 to –1)	–2 (–2 to –1)	–1 (–2 to –1)	–1 (–1 to –1)	–1 (–1 to –1)	–1 (–1 to –1)	–1 (–1 to 0)	–1 (–1 to 0)	0 (0–0)
Reader 2	–2 (–2 to –2)	–2 (–2 to –1)	–1.5 (–2 to –1)	–1 (–2 to –1)	–1 (–1 to –1)	–1 (–1 to –1)	–1 (–1 to 0)	–1 (–1 to 0)	–1 (–1 to 0)	0 (0–0)
Reader 3	–2 (–2.75 to –2)	–2 (–3 to –2)	–2 (–2 to –1)	–1 (–2 to –1)	–1 (–1 to –1)	–1 (–1 to –1)	–1 (–1 to –1)	–1 (–1 to –1)	–1 (–1 to –1)	0 (0–0)
Reader 4	–2 (–2 to –2)	–2 (–2 to –2)	–1 (–2 to –1)	–1 (–2 to –1)	–1 (–1 to –1)	–1 (–1 to –1)	–1 (–1 to –1)	–1 (–1 to –1)	–1 (–1 to 0)	0 (–0.75 to 0)

Note.—Data are presented as median qualitative image analysis scores; data in parentheses are interquartile range. QIR is an iterative reconstruction algorithm from Siemens Healthcare. T3D = polychromatic images at photon-counting detector CT.

ences in CT attenuation were computationally calculated for the whole image volume (22). Subtraction maps were calculated between QIR 1–4 and QIR-off. A detailed description of the method can be found in Appendix E1 (online).

### Qualitative Analysis

Qualitative analyses were performed independently by four readers (A.L., in training with 1 year of experience in CT; T.S., in training with 3 years of experience in CT; A.E., with 9 years of experience in CT; and M.E., with 9 years of experience in CT) in a randomized manner within an interval of 4 weeks. Readers were blinded both to imaging parameters and patient details.

The two junior readers rated the qualitative image quality parameters and all four readers rated lesion conspicuity. Reconstructions were linked so that identical anatomic levels could be evaluated during scrolling. The readers were allowed to adjust window settings and scroll and zoom images according to their personal preferences. No time limit was set for image review.

As recommended elsewhere (23), two five-point Likert scales were used to score overall image quality, image artifacts, and diagnostic confidence. A score of 5 indicated the best rating and scores below 3 were considered unacceptable (Appendix E1 [online]).

Furthermore, as previously suggested (24), a comparative scale was used to rank image noise, texture, and lesion conspicuity. A score of 0 was given for the best reconstruction; –1, slightly inferior (no influence on diagnosis); –2, mildly inferior (possible influence on diagnosis); –3, moderately inferior (probable influence on diagnosis); and –4, markedly inferior (impairing diagnosis). Scores could be used more than once if reconstructions were judged to be equivalent. Lesion conspicuity was rated in patients with hypodense liver lesions ( $n = 18$ ).

### Statistical Analysis

Sample size was comparable to previous studies (20). Interreader agreement of qualitative image quality scores was quantified with Krippendorff  $\alpha$  coefficients by using the following scale: 0–.20, poor agreement; .21–.40, fair agreement; .41–.60, moderate agreement; .61–.80, substantial agreement; and .81–1.00, almost perfect agreement.

Differences in the distribution of qualitative image quality scores between all reconstructions were initially checked with Friedman tests. Then, post hoc pairwise Wilcoxon signed-rank tests with a Benjamini-Hochberg correction for multiple comparisons were conducted to identify specific differences between the different reconstructions.

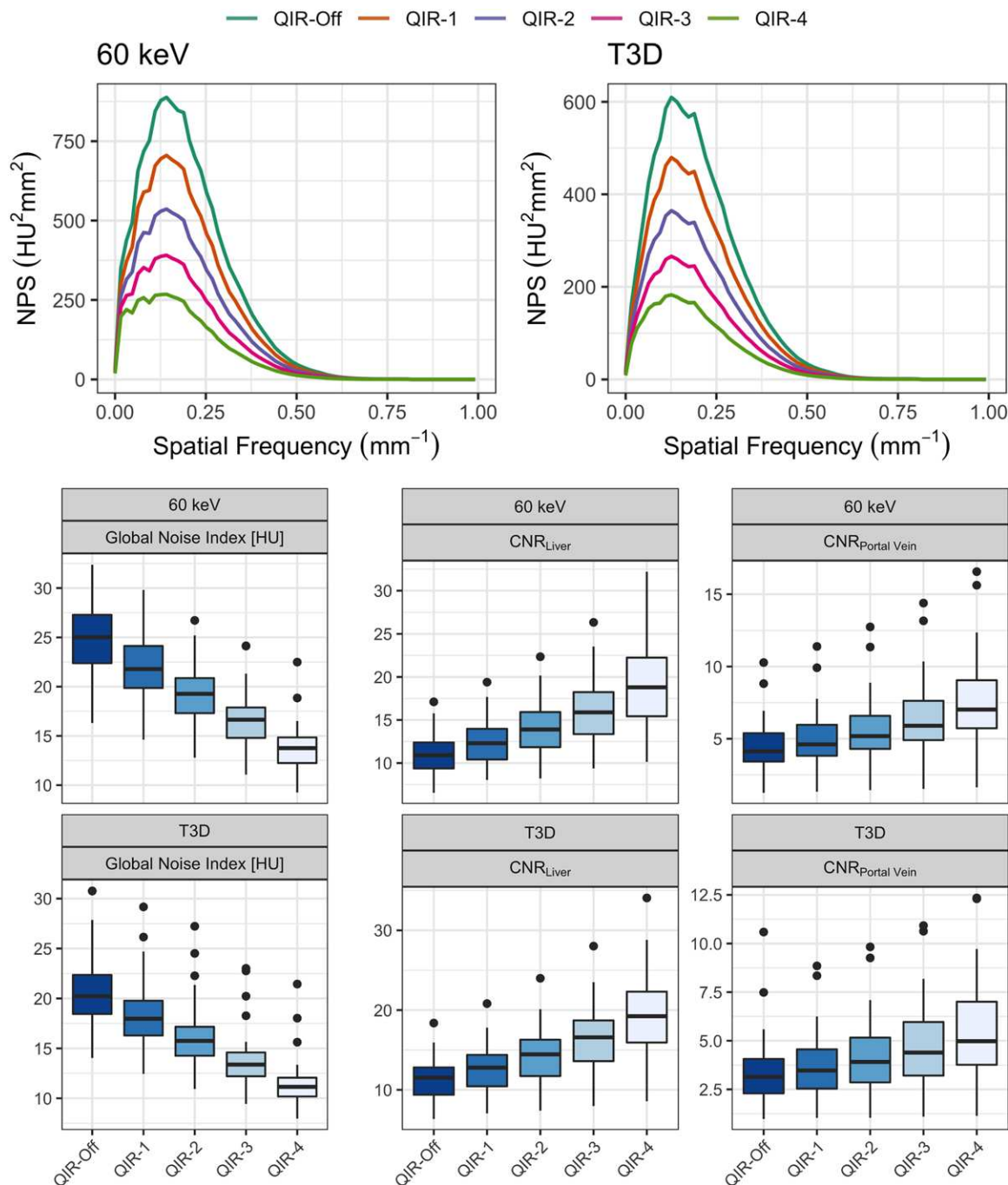


**Figure 2:** Quantitative image quality. Upper graphs show noise power spectrum (NPS) curves for 60 keV and polychromatic images at photon-counting detector CT (T3D) and all reconstructions. Note the similar shape of all curves except for the height. A reduction in height indicates a reduction in noise. Lower graphs show boxplots of the global noise index and contrast-to-noise ratio (CNR). The line in the box shows that the median, lower, and upper hinges correspond to the first and third quartiles. The upper and lower whiskers extend from the hinge to the largest and smallest value no farther than  $1.5 \times$  interquartile range from the hinge. QIR is an iterative reconstruction algorithm from Siemens Healthcare.

Mean differences in quantitative image quality scores and attenuation values between all reconstructions were initially checked with one-way repeated measures analyses of variance. Then, post hoc pairwise paired  $t$  tests with a Benjamini-Hochberg correction for multiple comparisons were conducted.

Two-tailed  $P$  values less than .05 were considered to indicate statistical significance. Wherever appropriate, CIs were provided. Quantitative variables are shown as means  $\pm$  standard deviation whereas qualitative variables are shown as medians with interquartile ranges. All statistical analyses were performed by one author (T.S.) with the statistical

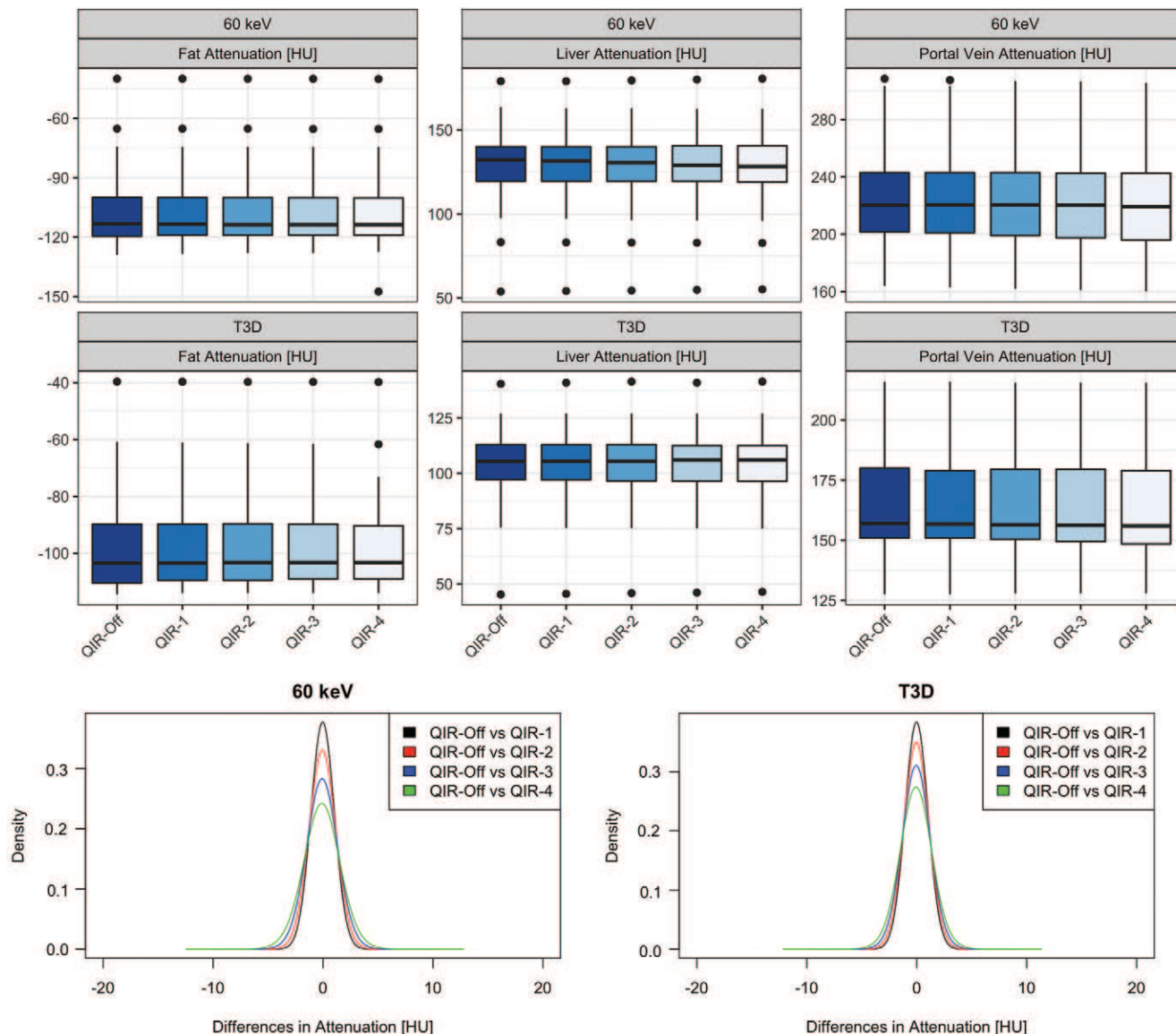


**Figure 3:** CT attenuation as a function of reconstruction. Overview of region-of-interest–based (upper two rows) and voxel-wise (bottom row) CT attenuation measurements. The box plots depict the distribution of the mean attenuation of anatomic structures among all 50 patients. Note the identical shape of the boxplots across all reconstructions indicating that the mean attenuation within anatomic structures (fat, liver portal vein) remained stable. In the bottom row, a density plot of the distribution of the difference in attenuation between all levels of QIR (Siemens Healthcare) and QIR-off is shown. Specifically, the curves shown in the graph represent the averaged data from all 50 patients. Most voxels cluster around 0, which indicates that CT attenuation stability is provided on a voxel-wise basis across all sections of an examination, regardless of the choice of reconstruction. T3D = polychromatic images at photon-counting detector CT.

software (R version 4.0.2; R Foundation for Statistical Computing, <https://www.R-project.org/>)

## Results

### Study Cohort

Fifty patients were included in the study. No patient was excluded (Fig 1).

### Quantitative Analysis

**Phantom.**—For the NPS, a maximum difference of 0.01 per millimeter was found for average spatial frequency and peak spatial frequency among all reconstructions (Table 2, Fig

2). From QIR-off to QIR-4, noise magnitude had a 46% reduction.

**Patients.**—For both 60 keV and T3D, global noise index was reduced from QIR-off to QIR-4 by 45% (95% CI: 44.7, 45.2) and 44% (95% CI: 43.8, 45.1), respectively ( $P < .001$  for each comparison of QIR 1, 2, 3, or 4 vs QIR-off; Table 2, Fig 2).

Liver CNR improved both for 60 keV and T3D from QIR-off to QIR-4 by 74% (95% CI: 71.9, 75.8) and 69% (95% CI: 66.2, 71.1), respectively (60 keV:  $P < .001$  to .04 for QIR 1–4 vs QIR-off; T3D:  $P = .10$  for QIR-1 vs QIR-off and  $P < .001$  for QIR 2, 3, and 4 vs QIR-off; Table 2, Fig 2).



Portal vein CNR improved both for 60 keV (QIR-1 vs QIR-off,  $P = .23$ ; QIR-2 vs QIR-off,  $P = .01$ ; QIR-3 and QIR-4 vs QIR-off,  $P < .001$ ) and T3D (QIR-1 and QIR-2 vs QIR-off,  $P = .06$ –.41; QIR-3 and QIR-4 vs QIR-off,  $P < .001$ ) from QIR-off to QIR-4 by 70% (95% CI: 68, 71.4) and 64% (95% CI: 62.5, 66), respectively (Table 2, Fig 2).

For fat and liver, we found no evidence of differences in CT attenuation between reconstructions for 60 keV and T3D (60 keV,  $P = .84$ ; T3D,  $P = .79$ ). For portal vein, differences were found between reconstructions both for 60 keV and T3D. Specifically, for 60 keV and T3D, the mean attenuation in the portal vein ranged from  $223 \text{ HU} \pm 34.2$  (60 keV) and  $163 \text{ HU} \pm 21.3$  (T3D) for QIR-off to  $221 \text{ HU} \pm 34.8$  (60 keV) and  $162 \text{ HU} \pm 21.4$  (T3D) for QIR-4, with statistically significant differences between the reconstructions (60 keV,  $P = .001$ –.005; T3D,  $P < .001$  to .002; Table 2, Fig 3).

Regarding voxel-wise differences in CT attenuation, a maximum mean difference in CT attenuation of 0.1 HU between QIR-off and a given QIR reconstruction (QIR-4 at 60 keV) was found (Table 2, Fig 3). At higher levels of QIR, more voxels showed larger deviations in attenuation compared with QIR-off than lower levels of QIR. This was shown by the standard deviation of the bell curves, which increased slightly at higher levels of QIR compared with lower levels of QIR (Fig 3). This effect can be explained by the improved image noise reduction at high levels of QIR. In addition, subtraction maps (Fig E2 [online]) demonstrated that the spatial distribution of attenuation differences between QIR and QIR-off reconstructions differed between homogeneous areas and anatomic edges (25). This effect increased with increasing QIR strength, as indicated by the accentuated edges (eg, the vertebra) at QIR-4.

### Qualitative Analysis

An overview of the results is given in Table 3 and Figure E3 (online). Representative image examples are provided in Figures 4–6. Interreader agreement was high between readers 1 and 2 for the metrics' overall image quality, image artifacts, diagnostic confidence, image noise, and texture ( $\alpha$  values ranged from .83 for overall image quality to .97 for image noise and texture). For lesion conspicuity, interreader agreement between all four readers was substantial ( $\alpha = .7$ ).

For both image types, both readers, and all categories (overall image quality, artifacts and diagnostic confidence, image noise, and texture), scores improved with higher levels of QIR, whereby QIR-4 outperformed all other reconstructions (all,  $P < .001$  to .01).

For lesion conspicuity, the four readers rated QIR-4 superior to other reconstructions (all,  $P < .001$  to .04) with scores ranging from  $-2$  (interquartile range,  $-2.75$  to  $-2$ ) to  $0$  (interquartile range,  $0$ – $0$ ) for 60 keV and  $-2$  (interquartile range,  $-3$  to  $-2$ ) to  $0$  (interquartile range,  $0$ – $0$ ) for T3D from QIR-off to QIR-4, respectively.

### Discussion

An iterative reconstruction algorithm (QIR; Siemens) was introduced with the clinical implementation of photon-counting

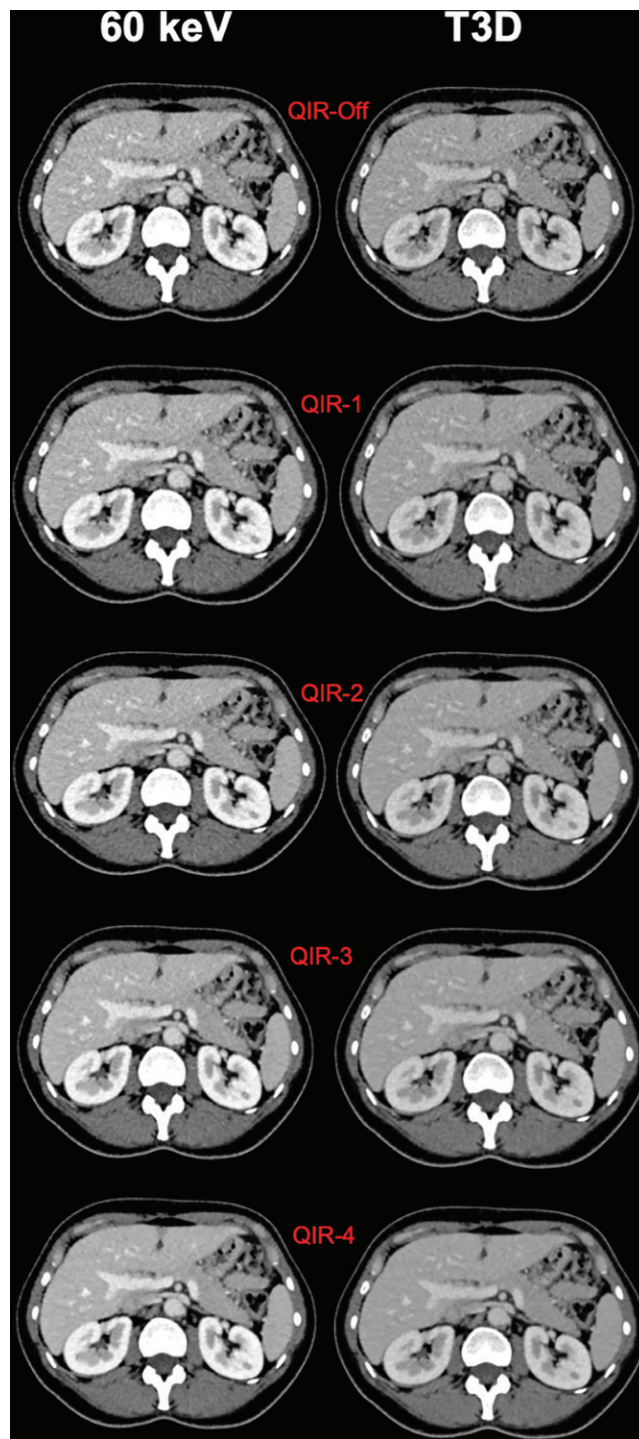


**Figure 4:** Representative axial CT images in a 41-year-old woman with neuroendocrine tumor of the appendix. Images are in the upper abdomen as a function of reconstruction for 60 keV and polychromatic images at photon-counting detector CT (T3D). Note the reduction in image noise with higher QIR (Siemens Healthcare) strength without visible changes in image noise texture. T3D = polychromatic images at photon-counting detector CT.

detector (PCD) CT. Our study investigated the image quality and the optimal strength level of QIR for virtual monoenergetic images and polychromatic images (T3D) in a phantom and patients in portal venous abdominal PCD CT. We found that the highest strength level of QIR improved objective and subjective

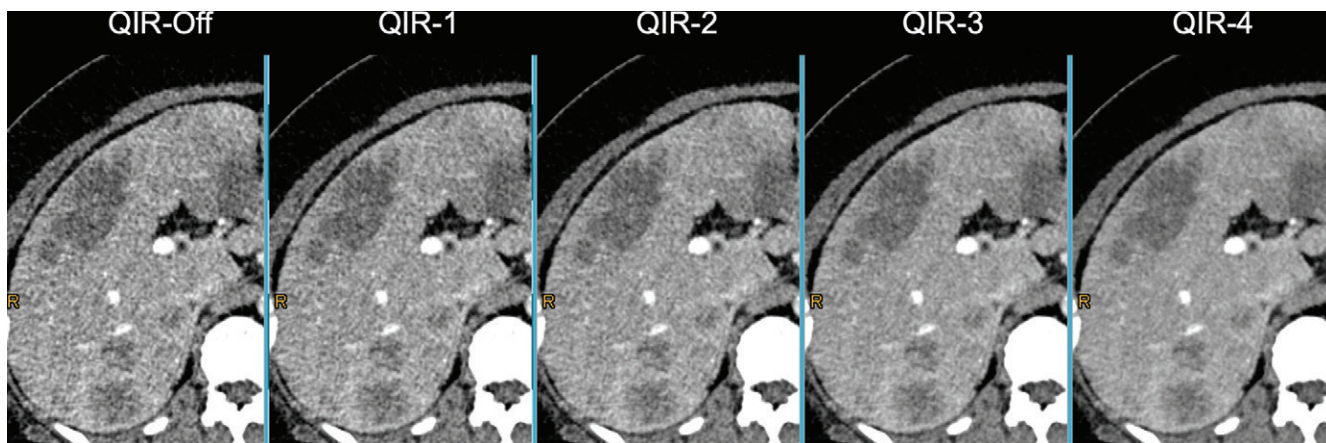


**Figure 5:** Axial CT images depict the liver of a 46-year-old woman with epithelioid hemangioendothelioma as a function of reconstruction for 60-keV monoenergetic images with representative examples of focal liver lesions. Note the reduction in image noise and improvement in lesion conspicuity at higher levels of iterative reconstruction (QIR; Siemens Healthcare).

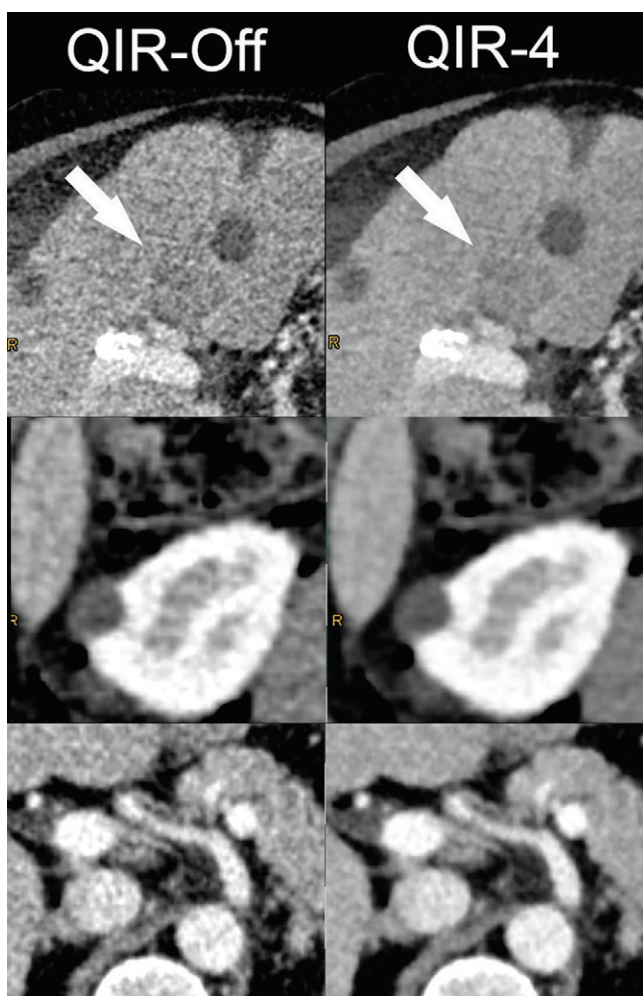


**Figure 6:** Axial CT images depicting the liver (top row) with washout of a hepatocellular carcinoma (arrows), a cortical renal cyst (middle row), and the celiac trunk (bottom row) reconstructed with QIR (Siemens Healthcare)-off (left column) and QIR-4 (right column) show a representative comparison of QIR-off versus QIR-4. Note the substantial reduction in image noise using QIR-4.

image quality compared with QIR-off with a reduction of image noise by 45% and 44% (each,  $P < .001$ ) and an improvement of contrast-to-noise ratio in the liver and portal vein by 74% and 70% and 69% and 64% for virtual monoenergetic images and T3D, respectively ( $P < .001$  for QIR-4 vs QIR-off). No evidence of difference was found for image texture and CT attenuation values among reconstructions (maximum deviation of 0.01 per millimeter spatial frequency and maximum mean attenuation difference of 2 HU). The results of our human reader study suggested improved subjective image quality and liver lesion conspicuity by using higher strength levels of QIR. On the basis of our findings, we recommend a QIR strength of 4 for clinical use in abdominal portal venous PCD CT.

Since their introduction in 2009, several IRs have been developed that enabled radiation dose and/or image noise reduction compared with filtered back projection (13,14). Current IRs designed for energy-integrating detector CT, however, cannot be used in PCD CT (13) because of the more complex data structure of PCD CT. First, multienergy data are inherently available and, second, additional detector elements can be deployed depending on the scan settings. These variations in image acquisition and additional differences in the noise model underlying PCD CT have a central role in image reconstruction. A further reconstruction challenge encountered in PCD CT is that image reconstruction and the step of material decomposition are not performed concurrently. This implies an information loss that cannot be compensated for with current IRs (13). Because of these challenges, QIR has been specifically tailored toward the requirements of PCD CT.

Image noise texture has a major effect on the perceived image quality. Previous IRs designed for energy-integrating detector CT have been shown to alter the noise frequency distribution. Specifically, central noise frequency shifted to lower values which caused a change in image texture and appearance (22,26–29). Our NPS analysis demonstrated that QIR was not affected by these previous limitations because similar average and peak noise frequencies were observed among all reconstructions. Consequently, QIR reduced noise

without affecting noise texture. This was also reflected by the improved subjective image quality for high levels of QIR compared with QIR-off. In our subjective analysis, lesion conspicuity of hypodense liver lesions was emphasized. Four independent readers with different experience levels rated significantly higher conspicuity scores for QIR-4 compared with the other reconstructions.

Nevertheless, the spatial distribution of attenuation differences between QIR and QIR-off reconstructions differed between homogeneous areas and anatomic edges. The general philosophy of QIR is to resemble the modulation transfer function of weighted filtered back projection as closely as possible. Therefore, QIR minimally increases sharpness at the edges between, for example, soft tissue and bone, which leads to a minimal difference in attenuation that is visible in the subtraction maps. However, these changes can be considered minimal because of the low magnitude of this effect.

Another important metric in quantitative analysis is CT attenuation stability. We investigated the effect of QIR strengths on mean CT attenuation with both a region-of-interest-based approach and a fully computational approach. Importantly, the computational approach measured attenuation differences on a whole-volume, voxel-wise basis. Both approaches confirmed that mean CT attenuation remained unaffected by QIR. This indicates that CT attenuation can be used for quantitative analysis independent of QIR strength level.

Our study had several limitations. First, this was a single-center study with a limited number of patients. Second, because of the heterogeneous patient cohort and the limited number of focal liver lesions, the diagnostic performance of various reconstructions was not assessed. Third, we did not assess the radiation dose reduction potential of QIR. Fourth, we were not able to compare QIR to other IRs because they were not available for PCD CT.

In conclusion, an iterative reconstruction algorithm (QIR; Siemens Healthcare) at a strength level of 4 performed best for quantitative and qualitative image quality as well as the conspicuity of liver lesions without affecting noise texture or CT attenuation in abdominal portal venous photon-counting detector CT. Future studies should assess the effect of QIR on diagnostic accuracy and its potential for radiation dose reduction. In particular, these studies should aim to assess low-contrast detectability with QIR while accounting for multiple features including size, shape, and scan parameters.

**Author contributions:** Guarantors of integrity of entire study, **T.S., H.A., A.E.**; study concepts/study design or data acquisition or data analysis/interpretation, all authors; manuscript drafting or manuscript revision for important intellectual content, all authors; approval of final version of submitted manuscript, all authors; agrees to ensure any questions related to the work are appropriately resolved, all authors; literature research, **T.S., A.L., M.E., K.H., R.R., H.A., A.E.**; clinical studies, **T.S., D.N., M.E., H.A., A.E.**; experimental studies, **T.S.**; statistical analysis, **T.S.**; and manuscript editing, all authors

**Disclosures of conflicts of interest:** **T.S.** No relevant relationships. **A.L.** No relevant relationships. **D.N.** No relevant relationships. **M.E.** No relevant relationships. **C.R.** No relevant relationships. **V.M.** No relevant relationships. **K.H.** No relevant relationships. **R.R.** Employed by Siemens Healthcare; patents for iterative reconstruction techniques; stock/stock options, Siemens and Siemens Healthineers. **H.A.** No relevant relationships. **A.E.** disclosed no relevant relationships.

## References

- Sartoretti T, Eberhard M, Rüschoff JH, et al. Photon-counting CT with tungsten as contrast medium: Experimental evidence of vessel lumen and plaque visualization. *Atherosclerosis* 2020;310:11–16.
- Yu Z, Leng S, Li Z, et al. How Low Can We Go in Radiation Dose for the Data-Completion Scan on a Research Whole-Body Photon-Counting Computed Tomography System. *J Comput Assist Tomogr* 2016;40(4):663–670.
- Willemink MJ, Persson M, Pourmorteza A, Pelc NJ, Fleischmann D. Photon-counting CT: Technical Principles and Clinical Prospects. *Radiology* 2018;289(2):293–312.
- Rajagopal JR, Farhadi F, Solomon J, et al. Comparison of Low Dose Performance of Photon-Counting and Energy Integrating CT. *Acad Radiol* 2021;28(12):1754–1760.
- Lell MM, Kachelrieß M. Recent and Upcoming Technological Developments in Computed Tomography: High Speed, Low Dose, Deep Learning, Multienergy. *Invest Radiol* 2020;55(1):8–19.
- Zhou W, Michalak GJ, Weaver JM, et al. A Universal Protocol for Abdominal CT Examinations Performed on a Photon-Counting Detector CT System: A Feasibility Study. *Invest Radiol* 2020;55(4):226–232.
- Muenzel D, Bar-Ness D, Roessl E, et al. Spectral Photon-counting CT: Initial Experience with Dual-Contrast Agent K-Edge Colonography. *Radiology* 2017;283(3):723–728.
- Symons R, Pourmorteza A, Sandfort V, et al. Feasibility of Dose-reduced Chest CT with Photon-counting Detectors: Initial Results in Humans. *Radiology* 2017;285(3):980–989.
- Pourmorteza A, Symons R, Sandfort V, et al. Abdominal Imaging with Contrast-enhanced Photon-counting CT: First Human Experience. *Radiology* 2016;279(1):239–245.
- Si-Mohamed SA, Sigovan M, Hsu JC, et al. In Vivo Molecular K-Edge Imaging of Atherosclerotic Plaque Using Photon-counting CT. *Radiology* 2021;300(1):98–107.
- Kwan AC, Pourmorteza A, Stutman D, Bluemke DA, Lima JAC. Next-Generation Hardware Advances in CT: Cardiac Applications. *Radiology* 2021;298(1):3–17.
- Nowak T, Eberhard M, Schmidt B, et al. Bone Mineral Density Quantification from Localizer Radiographs: Accuracy and Precision of Energy-integrating Detector CT and Photon-counting Detector CT. *Radiology* 2021;298(1):147–152.
- Willemink MJ, Noël PB. The evolution of image reconstruction for CT—from filtered back projection to artificial intelligence. *Eur Radiol* 2019;29(5):2185–2195.
- Mileto A, Guimaraes LS, McCollough CH, Fletcher JG, Yu L. State of the Art in Abdominal CT: The Limits of Iterative Reconstruction Algorithms. *Radiology* 2019;293(3):491–503.
- Brady SL, Trout AT, Somasundaram E, Anton CG, Li Y, Dillman JR. Improving Image Quality and Reducing Radiation Dose for Pediatric CT by Using Deep Learning Reconstruction. *Radiology* 2021;298(1):180–188.
- Mileto A, Zamora DA, Alessio AM, et al. CT Detectability of Small Low-Contrast Hypoattenuating Focal Lesions: Iterative Reconstructions versus Filtered Back Projection. *Radiology* 2018;289(2):443–454.
- Solomon J, Marin D, Roy Choudhury K, Patel B, Samei E. Effect of Radiation Dose Reduction and Reconstruction Algorithm on Image Noise, Contrast, Resolution, and Detectability of Subtle Hypoattenuating Liver Lesions at Multidetector CT: Filtered Back Projection versus a Commercial Model-based Iterative Reconstruction Algorithm. *Radiology* 2017;284(3):777–787.
- Ferda J, Vendiš T, Flohr T, et al. Computed tomography with a full FOV photon-counting detector in a clinical setting, the first experience. *Eur J Radiol* 2021;137:109614.
- Euler A, Higashigaito K, Mergen V, et al. High-Pitch Photon-Counting Detector Computed Tomography Angiography of the Aorta: Intraindividual Comparison to Energy-Integrating Detector Computed Tomography at Equal Radiation Dose. *Invest Radiol* 2021. 10.1097/RLI.0000000000000816. Published online August 4, 2021.
- Parakh A, Cao J, Pierce TT, Blake MA, Savage CA, Kambadakone AR. Sinogram-based deep learning image reconstruction technique in abdominal CT: image quality considerations. *Eur Radiol* 2021;31(11):8342–8353.
- Christianson O, Winslow J, Frush DP, Samei E. Automated Technique to Measure Noise in Clinical CT Examinations. *AJR Am J Roentgenol* 2015;205(1):W93–W99.

22. Steuwe A, Weber M, Bethge OT, et al. Influence of a novel deep-learning based reconstruction software on the objective and subjective image quality in low-dose abdominal computed tomography. *Br J Radiol* 2021;94(1117):20200677.
23. Wichmann JL, Hardie AD, Schoepf UJ, et al. Single- and dual-energy CT of the abdomen: comparison of radiation dose and image quality of 2nd and 3rd generation dual-source CT. *Eur Radiol* 2017;27(2):642–650.
24. Jensen CT, Liu X, Tamm EP, et al. Image Quality Assessment of Abdominal CT by Use of New Deep Learning Image Reconstruction: Initial Experience. *AJR Am J Roentgenol* 2020;215(1):50–57.
25. Guleng A, Bolstad K, Dalehaug I, Flatabø S, Aadnevik D, Pettersen HES. Spatial Distribution of Noise Reduction in Four Iterative Reconstruction Algorithms in CT-A Technical Evaluation. *Diagnostics (Basel)* 2020;10(9):E647.
26. Singh R, Digumarthy SR, Muse VV, et al. Image Quality and Lesion Detection on Deep Learning Reconstruction and Iterative Reconstruction of Submillisievert Chest and Abdominal CT. *AJR Am J Roentgenol* 2020;214(3):566–573.
27. Karmazyn B, Liang Y, Ai H, et al. Optimization of hybrid iterative reconstruction level in pediatric body CT. *AJR Am J Roentgenol* 2014;202(2):426–431.
28. Nelson RC, Feuerlein S, Boll DT. New iterative reconstruction techniques for cardiovascular computed tomography: how do they work, and what are the advantages and disadvantages? *J Cardiovasc Comput Tomogr* 2011;5(5):286–292.
29. Schaller F, Sedlmair M, Raupach R, Uder M, Lell M. Noise Reduction in Abdominal Computed Tomography Applying Iterative Reconstruction (ADMIRE). *Acad Radiol* 2016;23(10):1230–1238.

## Erratum

**Originally published in:**

<https://doi.org/10.1148/radiol.211931>

Quantum Iterative Reconstruction for Abdominal Photon-counting Detector CT Improves Image Quality

Thomas Sartoretti, Anna Landsmann, Dominik Nakhostin, Matthias Eberhard, Christian Roeren, Victor Mergen, Kai Higashigaito, Rainer Raupach, Hatem Alkadhi, André Euler

**Erratum in:**

<https://doi.org/10.1148/radiol.229013>

An error appeared in Figure 2: the y-axis on the upper left of the figure should be labeled as **0, 200, 400, 600**.